Advances in Aircraft and Spacecraft Science, *Vol. 12, No. 4 (2025) 291-313*
https://doi.org/10.12989/aas.2025.12.4.291

Thermal response of functionally graded sandwich plates using a semi-analytical approach

Rohan S. Bhagat, Sandeep S. Pendhari*, Sunil S. Yadav and Yuwaraj M. Ghugal

Department of Structural Engineering, Veermata Jijabai, Technological Institute, H. R. Mahajani Marg, Matunga, Mumbai, 400019, Maharashtra, India

(Received June 25, 2025, Revised September 11, 2025, Accepted September 12, 2025)

Abstract. This paper presents a semi-analytical method for analysing the through-thickness stress and displacement distributions in simply supported functionally graded (FG) sandwich plates under thermal loading. The formulation is based on theory of elasticity equations leading to ordinary differential equations (ODEs) with a two-point boundary value problem approach. In this method ad-hoc assumptions are not made on displacements and stresses. The material properties (modulus of elasticity, coefficient of thermal expansion and thermal conductivity) vary according to a power law in the thickness direction, while the Poisson's ratio is kept constant throughout the depth of the plate. The plate is subjected to a temperature gradient across its thickness using Fourier heat conduction law, and the thermal response of the FG sandwich plate is evaluated in terms of stresses and displacements. Semi-analytical formulation in this study is validated for pure FGM plate under thermal load and results are compared with those of higher order theory to establish the efficacy and efficiency of the presented method. The study provides a comprehensive behaviour of FG sandwich plates under thermal loading, highlighting the importance of accurate modelling and analysis. The results presented in this theory can be served as benchmark solutions in absence of exact solutions.

Keywords: exact thermal profile; heat conduction; initial value problem; Power law; power law; sandwich FGM; semi-analytical method

1. Introduction

Composite laminated structures are vital in engineering industries due to their superior mechanical properties, but due to mismatch in material properties at layer interfaces can result in interlaminar stress concentration and delamination (Jones 1975). Functionally graded materials (FGMs), with gradually changing properties, addressed this issue by varying the volume fractions of constituent materials (Shiota and Miyamoto 1997). This results in smoother stress distributions, making FGMs robust, thermally resilient, reliable, and durable.

The objective of this research is to provide a solution for thermal loading for which the FGM material is invented (Koizumi 1997). In a three-layered sandwich structure with a ceramic core and FGM outer plates with metal faces, the thermal resistivity benefits are significant. The ceramic core provides excellent thermal insulation and high-temperature resistance. The FGMs create a smooth gradient from the ceramic core to the metal surfaces, reducing thermal stresses from abrupt

*Corresponding author, Ph.D., E-mail: sspendhari@st.vjti.ac.in

http://www.techno-press.org/aas/8 ISSN: 2287-528X (Print), 2287-5271 (Online)

material changes and enhancing overall thermal resistance (Garg *et al.* 2021, Sankar and Tzeng 2002). Metal faces add structural strength and help in heat dissipation due to their higher thermal conductivity, reducing localized thermal stresses. This makes the structure ideal for high-temperature applications like spacecraft re-entry. Adjusting the material gradient optimizes thermal resistance and mechanical properties for specific uses.

Dadashi and Mahdiabadi (2024) developed an analytical model to investigate the free vibration of sandwich nano-shells with various FGM configurations, employing first-order shear deformation and modified nonlocal elasticity theories. Their results revealed that the metal-core configuration yields the highest frequencies, while increasing nonlocal parameter and side-to-thickness ratio reduce the frequency, providing valuable insights for the design of nano-shell structures in nanodevices and energy harvesting applications. Similarly, Madanouei and Mahdiabadi (2024) proposed a nonlinear energy sink (NES) strategy to mitigate free and forced vibrations in nonlinear FG shear-deformable beams, combining higher-order shear deformation theories with advanced numerical methods. Through genetic algorithm optimization, their study achieved up to 92.5% reduction in vibration amplitude and demonstrated the significant influence of FG material distribution and shear deformation theories on the optimal design of NES systems. Together, these works advance understanding of vibration behaviour and control in FG structures, offering potential for improved performance in aerospace, energy, and structural applications.

Several researchers have contributed significantly to the modelling and analysis of FGM and functionally graded porous (FGP) plates under thermo-mechanical loading conditions. Benguediab *et al.* (2023) presented displacement model incorporating shear deformation effects to study the static behaviour of FGM macro and nano-plates using both local and non-local elasticity theories. The influence of geometry, scale effects, and material index is examined. Zohra *et al.* (2023) presented the analysis of FGP sandwich plates under various thermal loading condition accounting for porosity defects using power-law distribution. The effects of porosity distribution, sandwich configuration, aspect ratio, and boundary constraints on thermal buckling behaviour are studied. Benameur *et al.* (2023) conducted a comparative analysis between analytical and finite element approaches for the bending behaviour of porous FGM sandwich plates subjected to sinusoidal loading. Utilizing a refined shear deformation theory with five unknowns and eliminating the need for shear correction factors, the analytical solution and the FEM solution showed strong correlation, although the analytical model inherently predicted symmetric responses. Hamidi *et al.* (2015) presented the sinusoidal shear and normal deformations theory for thermomechanical bending of FGM sandwich plates with the face sheets modelled using power-law graded materials and a ceramic core. The effect of side-to-thickness ratio, aspect ratio, the volume fraction exponent, and the loading conditions on the thermo-mechanical response of functionally graded sandwich plates is investigated. Naghavi *et al.* (2022) proposed a finite strip method based on refined plate theory for static analysis of FG sandwich plate. Two configurations are analysed having FGM face sheets with a homogeneous core, and homogeneous face sheets with an FGM core.

Recent advances in the analysis of functionally graded and sandwich plates have focused on refined shear deformation and quasi-3D theories to capture bending and stability behaviours under complex conditions. Himeur *et al.* (2022) studied the coupled effects of loading, thickness stretching, and non-uniform Winkler-Pasternak foundations on FG plates, while Slimani *et al.* (2024) developed a novel quasi-3D refined theory considering porosity and thickness stretching for accurate bending responses. Yadav *et al.* (2022, 2023a,b) studies the bending behaviour of FG beams and Plates under mechanical loading. Chitour *et al.* (2024) analysed FG sandwich plates

using a hyperbolic quasi-3D theory with reduced unknowns to investigate sinusoidal loading effects. Tamrabet *et al.* (2023, 2024) extended these approaches by proposing higher-order and quasi-3D models for porous FG sandwich plates, including configurations with FGM face sheets, ceramic/metal-foam cores, and various porosity distributions. Their studies demonstrated the influence of parameters such as power-law index, porosity, aspect ratio, boundary conditions, elastic foundations, and in-plane loading on bending and buckling responses, with analytical solutions validated against existing benchmarks.

To address challenges in sandwich and composite plates under thermal loading, Kant *et al.* (2008) developed a semi-analytical method incorporating stress and displacement variables, starting from three-dimensional partial differential equations. Their findings showed that while thin plate deflection remains relatively unchanged along the depth, thick plate deflection varies significantly. Kulkarni and Pendhari (2021) further studied this method for static solutions of functionally graded simply supported plates using double Fourier series with trigonometric functions for primary variables, leading to a set of linear first-order ordinary differential equations (ODEs). This method maintains the fundamental relationship between stress, strain, and displacement fields, providing a robust and reliable analysis of laminated composites.

Three-dimensional (3D) solutions for transient thermal stress analyses of functionally graded material (FGM) panels have been investigated by many researchers (Hajlaoui *et al.* 2021, Li *et al.* 2014, Malek *et al.* 2020). The transient stresses for a rectangular, simply supported FGM plate with uniform temperature at the edges and time-dependent temperature or heat flux on the top and bottom surfaces were determined by Vel and Batra (2002, 2003), who examined a 3D transient heat conduction problem. Normal and transverse transient thermal shear stresses in functionally graded, simply supported rectangular plates exposed to partial heat supply were explored by Zenkour (2005). Additionally, 3D solutions for transient temperature and thermal stresses in simply supported FGM rectangular plates with nonuniform heat supply were provided by Tanigawa and Ootao (1999), who assumed exponential variation of properties in the thickness direction. A 3D thermomechanical analysis was conducted by Shao *et al.* (2007), who derived an analytical solution for time-dependent temperature and thermomechanical stresses in FG cylindrical panels using Laplace transforms and series solution methods for ordinary differential equations. The time-dependent response of sandwich plates with FGM cores was investigated by Alibeigloo and Shakeri (2007) using generalized coupled thermo-elasticity.

The issue of transient stress analysis in cracked FGM panels under thermal shock were examined by Zhi-He and Naotake (1994) with various crack types and obtained thermal stress intensity factors both analytically and numerically. The stress intensity factor for TiC/SiC FGM strips with an edge crack under transient thermal loading were studied by Jin and Paulino (2000). Based on higher-order layer wise theory and Sander theory, Pandey and Pradyumna (2018) present a finite element formulation for stress analysis of FGM sandwich plates and shell panels under thermal shock. Di Sciuva and Sorrenti (2021) employed the refined zigzag theory for FGM plates to analyse static flexure and free vibration behaviour under various boundary conditions providing accurate results of FGM sandwich plates. Neves *et al.* (2013) used higher-order shear deformation theory (HSDT) with a meshless technique for free vibration and buckling behaviour of FGM plates considering thickness stretching effect.

The literature review reveals a lack of exact solutions for functionally graded sandwich plates with material properties varying according to a power law with actual thermal profiles (heat conditions). Among the various methods, the novelty of semi-analytical method is in providing solutions that are remarkably close to the exact solutions. Based on the basic equations of linear

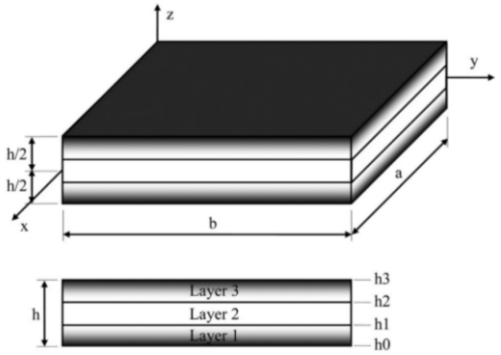

Fig. 1 Functionally graded sandwich plate geometry and co-ordinate system

theory of elasticity semi-analytical method is developed leading to a two-point boundary value problem which is solved using shooting method of numerical integration. The influence of stacking sequence of layers, aspect ratio (side/thickness), planar aspect ratio, and FG material inhomogeneity index on thermal response of FGM sandwich is examined. The results of semi-analytical method are compared with the refined shear deformation theory. This method offers an efficient alternative to exact solution and can be considered as a benchmark solution to validate other approximate solutions.

2. Mathematical formulation

The functionally graded sandwich plate consists of three layers with ceramic core and two FGM face sheets. The material properties, modulus of elasticity, coefficient of thermal expansion (α) and thermal conductivity (λ) are varying according to power law through the thickness of plate as given in Eqs. (1)-(3) (Sayyad and Ghugal 2021). Mathematical formulation of functionally graded sandwich plate is derived using semi-analytical method. A two-point boundary value problem is derived and converted to initial value problem.

$$E(z) = E_m + (E_c - E_m)V_c(z) \tag{1}$$

$$\alpha(z) = \alpha_m + (\alpha_c - \alpha_m)V_c(z) \tag{2}$$

$$\lambda(z) = \lambda_m + (\lambda_c - \lambda_m)V_c(z) \tag{3}$$

where the variation of constituent material $V_c(z)$ across the depth of plate is given as

$$V_c(z) = \left(\frac{z - h_0}{h_1 - h_0}\right)^k \quad \text{for} \quad z \in [h_0, h_1]$$

$$V_c(z) = 1 \quad \text{for} \quad z \in [h_1, h_2]$$

$$V_c(z) = \left(\frac{z - h_3}{h_2 - h_3}\right)^k \quad \text{for} \quad z \in [h_2, h_3]$$

where E_m and E_c are Young's moduli, α_m and α_c are coefficients of thermal expansion, λ_m and

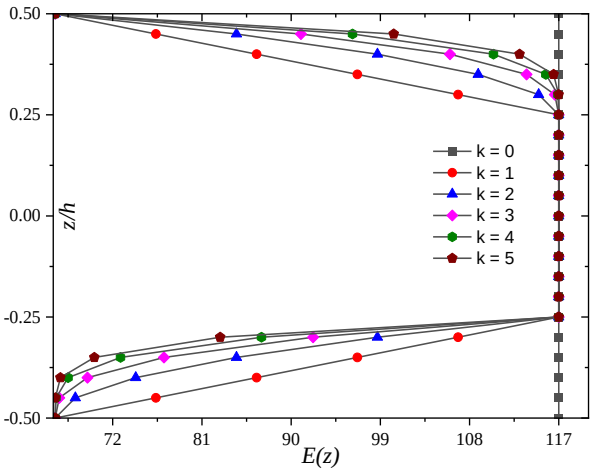

Fig. 2 Variation of elastic modulus of FGM sandwich plate for various power law indices, k

λ_c are coefficients of thermal conductivity of metal and ceramic, respectively and k is the power law index representing the inhomogeneity of FGM.

A linearly elastic rectangular simply supported FGM sandwich plate is shown in Fig. 1 with geometry and coordinate system. Face sheets (Layer 1 and 3) are of FGM material and core (Layer 2) is made up of ceramic. The plate is subjected to thermal load, $T(x, y)$ on top surface, and its variation through the thickness is applied according to Fourier law of heat conduction under steady state condition. The variation of elastic modulus according to power law across the thickness of FGM sandwich plate is presented in Fig. 2 for various power law indices k.

2.1 Solution for ordinary differential equations for heat conduction and constitutive relations

FGM's are primarily utilized in environments where structures are subjected to high temperatures. Consequently, precise evaluation of structural responses is crucial. This section focuses on the detailed formulation for the three-dimensional heat conduction equation. A thermal load and heat flux, as described in Eqs. (4) and (5), are considered, with the temperature values known only at the top and bottom surfaces of the laminate.

$$T(x, y, z) = \sum_{m,n=1}^{\infty} T(z) \sin\frac{m\pi x}{a} \sin\frac{n\pi y}{b} \tag{4}$$

$$q(x, y, z) = \sum_{m,n=1}^{\infty} q(z) \sin\frac{m\pi x}{a} \sin\frac{n\pi y}{b} \tag{5}$$

A governing three-dimensional (3D) Fourier heat conduction law for steady state condition without internal heat dissipation is given by Boley and Weiner (1960), Carslaw and Jaeger (1947), Ingersoll *et al.* (1948), Özışık (1989) as follows

$$\lambda(z)\frac{\partial^2 T}{\partial x^2} + \lambda(z)\frac{\partial^2 T}{\partial y^2} + \lambda(z)\frac{\partial^2 T}{\partial z^2} = 0 \tag{6}$$

Also, the Fourier heat conduction law in terms of heat fluxes in x, y and z directions is given as below

$$\frac{\partial q_x}{\partial x}+\frac{\partial q_y}{\partial y}+\frac{\partial q_z}{\partial z}=0 \tag{7}$$

From which we get

$$\frac{\partial q_z}{\partial z}=-\left(\frac{\partial q_x}{\partial x}+\frac{\partial q_y}{\partial y}\right) \tag{8}$$

where heat fluxes (q_x, q_y, q_z) are given by

$$q_x=-\lambda(z)\frac{\partial T}{\partial x};\quad q_y=-\lambda(z)\frac{\partial T}{\partial y};\quad q_z=-\lambda(z)\frac{\partial T}{\partial z} \tag{9}$$

Substituting Eqs. (9) into (8) we get Eq. (10)

$$\frac{\partial q_z}{\partial z}=-\left(\lambda(z)\frac{\partial^2 T}{\partial x^2}+\lambda(z)\frac{\partial^2 T}{\partial y^2}\right) \tag{10}$$

Substituting Eq. (4) into Eq. (10), we get

$$\frac{\partial q_z}{\partial z}=-\lambda(z)\left(\frac{m^2\pi^2}{a^2}+\frac{n^2\pi^2}{b^2}\right)T(z) \tag{11}$$

Now rearranging third of Eq. (9) gives

$$\frac{\partial T}{\partial z}=-\frac{q_z}{\lambda(z)} \tag{12}$$

Eqs. (11) and (12) are the given governing equations of two-point boundary value problem (BVP) of temperature field with the known temperature at the upper and lower surfaces of FG plate.

To form BVP, according to semi analytical method, three-dimensional (3D) strain-displacement relations, equilibrium equations, and constitutive relations for the thermo-elastic analysis of FGM sandwich plate are used. The strain-displacement relations are given as follows

$$\begin{aligned} &\varepsilon_x=\frac{\partial u}{\partial x}\ ; && \varepsilon_y=\frac{\partial v}{\partial y}; && \varepsilon_z=\frac{\partial w}{\partial z}\\ &\gamma_{xy}=\frac{\partial u}{\partial y}+\frac{\partial v}{\partial x}; && \gamma_{xz}=\frac{\partial u}{\partial z}+\frac{\partial w}{\partial x}; && \gamma_{yz}=\frac{\partial w}{\partial y}+\frac{\partial v}{\partial z} \end{aligned} \tag{13}$$

The thermoelastic constitutive relations for thermo-mechanical loading are given as follows

$$\begin{Bmatrix}\sigma_x\\ \sigma_y\\ \sigma_z\\ \tau_{xy}\\ \tau_{xz}\\ \tau_{yz}\end{Bmatrix}=\begin{bmatrix}C_{11}&C_{12}&C_{13}&0&0&0\\ C_{21}&C_{22}&C_{23}&0&0&0\\ C_{31}&C_{32}&C_{33}&0&0&0\\ 0&0&0&C_{44}&0&0\\ 0&0&0&0&C_{55}&0\\ 0&0&0&0&0&C_{66}\end{bmatrix}\begin{Bmatrix}\varepsilon_x-\alpha T\\ \varepsilon_y-\alpha T\\ \varepsilon_z-\alpha T\\ \gamma_{xy}\\ \gamma_{xz}\\ \gamma_{yz}\end{Bmatrix} \tag{14}$$

where $C_{ij}(i,j=1 \text{ to } 6)$ are stiffness coefficients in terms of elastic constants defined as follows

$$C_{11}=C_{22}=C_{33}=\frac{E(z)(1-\nu^2)}{(1-3\nu^2-2\nu^3)};\quad C_{44}=C_{55}=C_{66}=\frac{E(z)}{2(1+\nu)};$$
$$C_{12}=C_{21}=C_{13}=C_{31}=C_{23}=C_{32}=\frac{E(z)(\nu+\nu^2)}{(1-3\nu^2-2\nu^3)}. \tag{15}$$

The 3D stress equilibrium equations used are as follows.

$$\sigma_{ij,j}=0\ \ (i,j=x,y,z) \tag{16}$$

By using strain-displacement relations, equilibrium equations, and constitutive relations following set of six first order partial differential equations is obtained.

$$\frac{\partial u}{\partial z}=-\frac{\partial w}{\partial x}+\frac{\tau_{xz}}{C_{55}} \tag{17}$$

$$\frac{\partial v}{\partial z}=-\frac{\partial w}{\partial y}+\frac{\tau_{yz}}{C_{66}} \tag{18}$$

$$\frac{\partial w}{\partial z}=\frac{\sigma_z}{C_{33}}-\frac{C_{31}}{C_{33}}\frac{\partial u}{\partial x}-\frac{C_{32}}{C_{33}}\frac{\partial v}{\partial y}+\frac{\alpha T}{C_{33}}(C_{31}+C_{32}+C_{33}) \tag{19}$$

$$\begin{aligned}\frac{\partial \tau_{xz}}{\partial z}=&-\frac{\partial^2 u}{\partial x^2}\left(C_{11}-\frac{C_{13}C_{31}}{C_{33}}\right)-\frac{\partial^2 u}{\partial y^2}(C_{44})-\frac{\partial^2 v}{\partial x\partial y}\left(C_{12}+C_{44}-\frac{C_{13}C_{32}}{C_{33}}\right)\\&+\alpha\frac{\partial T}{\partial x}\left[C_{11}+C_{12}+C_{13}-\frac{C_{13}}{C_{33}}(C_{31}+C_{32}+C_{33})\right]-\frac{\partial \sigma_z}{\partial x}\left(\frac{C_{13}}{C_{33}}\right)\end{aligned} \tag{20}$$

$$\begin{aligned}\frac{\partial \tau_{yz}}{\partial z}=&-\frac{\partial^2 v}{\partial y^2}\left(C_{22}-\frac{C_{23}C_{32}}{C_{33}}\right)-\frac{\partial^2 v}{\partial x^2}(C_{44})-\frac{\partial^2 u}{\partial x\partial y}\left(C_{21}+C_{44}-\frac{C_{23}C_{31}}{C_{33}}\right)\\&+\alpha\frac{\partial T}{\partial y}\left[C_{21}+C_{22}+C_{23}-\frac{C_{23}}{C_{33}}(C_{31}+C_{32}+C_{33})\right]-\frac{\partial \sigma_z}{\partial y}\left(\frac{C_{23}}{C_{33}}\right)\end{aligned} \tag{21}$$

$$\frac{\partial \sigma_z}{\partial z}=-\frac{\partial \tau_{yz}}{\partial y}-\frac{\partial \tau_{xz}}{\partial x} \tag{22}$$

3. Numerical analysis

For numerical study pure FGM and FGM sandwich rectangular plates are considered. The simply supported boundary conditions are prescribed as follows

$$\begin{gathered}u=0 \text{ at } x=a/2 \text{ and } y=0\\ v=0 \text{ at } y=b/2 \text{ and } x=0\\ \tau_{xz}=\tau_{yz}=\sigma_z=0 \text{ at } z=\pm h/2.\end{gathered} \tag{23}$$

The solution for primary variables satisfying simply supported boundary conditions at four edges of plate is assumed in double trigonometric series as follows

$$u(x, y, z) = \sum_{m,n=1}^{\infty} u_{mn}(z) \cos\frac{m\pi x}{a} \sin\frac{n\pi y}{b} \tag{24}$$

$$v(x, y, z) = \sum_{m,n=1}^{\infty} v_{mn}(z) \sin\frac{m\pi x}{a} \cos\frac{n\pi y}{b} \tag{25}$$

$$w(x, y, z) = \sum_{m,n=1}^{\infty} w_{mn}(z) \sin\frac{m\pi x}{a} \sin\frac{n\pi y}{b} \tag{26}$$

$$\tau_{xz}(x, y, z) = \sum_{m,n=1}^{\infty} \tau_{xzmn}(z) \cos\frac{m\pi x}{a} \sin\frac{n\pi y}{b} \tag{27}$$

$$\tau_{yz}(x, y, z) = \sum_{m,n=1}^{\infty} \tau_{yzmn}(z) \sin\frac{m\pi x}{a} \cos\frac{n\pi y}{b} \tag{28}$$

$$\sigma_{z}(x, y, z) = \sum_{m,n=1}^{\infty} \sigma_{zmn}(z) \sin\frac{m\pi x}{a} \sin\frac{n\pi y}{b} \tag{29}$$

Substituting the solution given by Eqs. (24)-(29) into governing Eqs. (17)-(22) we get following coupled first order ordinary differential equations (ODEs)

$$\frac{du_{mn}(z)}{dz} = -\frac{m\pi}{a} w_{mn}(z) + \frac{\tau_{xzmn}(z)}{C_{55}} \tag{30}$$

$$\frac{\partial v_{mn}(z)}{\partial z} = -\frac{n\pi}{b} w_{mn}(z) + \frac{\tau_{yzmn}(z)}{C_{66}} \tag{31}$$

$$\frac{\partial w_{mn}(z)}{\partial z} = \frac{\sigma_{zmn}(z)}{C_{33}} + \frac{C_{31}}{C_{33}} u_{mn}(z)\frac{m\pi}{a} + \frac{C_{32}}{C_{33}} v_{mn}(z)\frac{n\pi}{b} + \frac{\alpha T(z)}{C_{33}}(C_{31} + C_{32} + C_{33}) \tag{32}$$

$$\begin{aligned}\frac{\partial \tau_{xz\,mn}(z)}{\partial z} &= u_{mn}(z)\ \frac{m^2\pi^2}{a^2}\left(C_{11} - \frac{C_{13}C_{31}}{C_{33}}\right) + u_{mn}(z)\frac{n^2\pi^2}{b^2}\left(C_{44}\right) \\ &\quad + v_{mn}(z)\frac{mn\pi^2}{ab}\left(C_{12} + C_{44} - \frac{C_{13}C_{32}}{C_{33}}\right) \\ &\quad + \alpha T(z)\frac{m\pi}{a}\left[C_{11} + C_{12} + C_{13} - \frac{C_{13}}{C_{33}}(C_{31} + C_{32} + C_{33})\right] - \sigma_{zmn}(z)\frac{m\pi}{a}\left(\frac{C_{13}}{C_{33}}\right)\end{aligned} \tag{33}$$

Table 1 Scheme for temperature variation by transforming BVP to IVP

Integration No.	Bottom Surface ($z=-h/2$)		Top Surface ($z=h/2$)	
	$T(z)$	$q(z)$	$T(z)$	$q(z)$
1	Known	0 (Assumed)	A_1	A_2
2	0 (Assumed)	1	B_1	B_2
Final	Known	B_2	T(known)	q

Table 2 Scheme for solving ODEs for stress and displacement by transforming BVP to IVP

Integ-	Bottom Surface ($z=-h/2$)						Top Surface ($z=h/2$)						Load
ration No.	u	v	w	τ_{xz}	τ_{yz}	σ_{zz}	u	v	w	τ_{xz}	τ_{yz}	σ_{zz}	Term
1	0	0	0	0	0	0	A_{11}	A_{12}	A_{13}	A_{14}	A_{15}	A_{16}	Include
2	1	0	0	0	0	0	A_{21}	A_{22}	A_{23}	A_{24}	A_{25}	A_{26}	Exclude
3	0	1	0	0	0	0	A_{31}	A_{32}	A_{33}	A_{34}	A_{35}	A_{36}	Exclude
4	0	0	1	0	0	0	A_{41}	A_{42}	A_{43}	A_{44}	A_{45}	A_{46}	Exclude
Final	A_{44}	A_{45}	A_{46}	0	0	0	$u(h)$	$v(h)$	$w(h)$	0	0	0	Include

$$\frac{\partial \tau_{yzmn}(z)}{\partial z} = v_{mn}(z)\frac{n^2\pi^2}{b^2}\left(C_{22}-\frac{C_{23}C_{32}}{C_{33}}\right)+v_{mn}(z)\frac{m^2\pi^2}{a^2}\left(C_{44}\right) + u_{mn}(z)\frac{mn\pi^2}{ab}\left(C_{21}+C_{44}-\frac{C_{23}C_{31}}{C_{33}}\right) + \alpha T(z)\tau_{yzmn}(z)\frac{n\pi}{b}\left[C_{21}+C_{22}+C_{23}-\frac{C_{23}}{C_{33}}\left(C_{31}+C_{32}+C_{33}\right)\right]-\sigma_{zmn}(z)\frac{n\pi}{b}\left(\frac{C_{23}}{C_{33}}\right) \tag{34}$$

$$\frac{\partial \sigma_{zmn}(z)}{\partial z} = \tau_{yzmn}(z)\frac{n\pi}{b}+\tau_{xzmn}(z)\frac{m\pi}{a} \tag{35}$$

System of Eqs. (30)-(35) is solved as BVP by using shooting method reported by Desai and Kant (2015) in conjunction with Runga-Kutta method for thermal and stress analysis which has been tabulated in Tables 1 and 2 where Tables 1 and 2 represent initial variables for temperature profile and stresses and displacements calculation respectively.

4. Numerical results and discussion

MATLAB codes are developed to obtain exact thermal profile and to perform displacement and stress analysis of pure FGM plate and FG sandwich plate using semi-analytical method.

4.1 Example 1: Pure FGM plate

Present formulation is validated for pure FG plates. For the numerical study, reference temperature at the lower and upper surfaces of the FG plate considered are 20°C and 300°C respectively. Material properties of FGM plate are given in Table 3. The thermoelastic bending analysis is conducted for FGM plate. The FGM consists of materials Titanium (Ti-6Al-4V) and

Table 3 Properties of material used in FG sandwich plate

Properties	Metal-Ti-6Al-4V	Ceramic-ZrO_2
E (GPa)	66.2	117
μ (Poisson's Ratio)	1/3	1/3
α (Coeff. of Thermal Expansion) 10^{-6}	10.3	7.11
Thermal Conductivity (W/m-k)	6.7	1.7

Table 4 Depth ordinates for different schemes

Ordinate	Scheme				
	1-0-1	1-1-1	1-2-1	2-1-2	1-3-1
h_0	$-h/2$	$-h/2$	$-h/2$	$-h/2$	$-h/2$
h_1	0	$-h/6$	$-h/4$	$-h/10$	$-3h/10$
h_2	0	$h/6$	$h/4$	$h/10$	$3h/10$
h_3	$h/2$	$h/2$	$h/2$	$h/2$	$h/2$

Zirconia (ZrO_2). Various power indices (k) have considered from metal (bottom) to ceramic (top) as a variation of material gradation across thickness direction. Convergence study is performed for complete flexural response. Based on convergence studies, convergence is observed with 20 steps of numerical integration through the thickness of plate. Results obtained are compared with Kulkarni and Pendhari (2021) to validate the present semi-analytical formulation. The displacements and stresses are normalized according Eq. (36) and presented in Table 5 and are found to be in close agreement with those of Kulkarni and Pendhari (2021). After the validation, the current formulation is applied to FGM sandwich plate for various lamination schemes. Here lamination schemes refer to the arrangement of core and FG layers which are described in Table 4 with reference to Fig. 1.

The displacements and stresses of pure FGM rectangular plate are normalised as follows

$$\bar{u} = \frac{100}{\alpha_b T_b S^3}\frac{u}{h} \qquad \bar{v} = \frac{100}{\alpha_b T_b S^3}\frac{v}{h} \qquad \bar{w} = \frac{100}{\alpha_b T_b S^4}\frac{w}{h} \qquad \bar{\sigma}_x = \frac{20\sigma_x}{E_b \alpha_b T_b S^2}$$

$$\bar{\sigma}_y = \frac{20\sigma_y}{E_b \alpha_b T_b S^2} \qquad \bar{\tau}_{xy} = \frac{20\tau_{xy}}{E_b \alpha_b T_b S^2} \qquad \bar{\tau}_{xz} = \frac{100\tau_{xz}}{E_b \alpha_b T_b S} \qquad \bar{\tau}_{yz} = \frac{100\,\tau_{yz}}{E_b \alpha_b T_b S} \tag{36}$$

where S is the side to thickness ratio (a/h) and subscript b indicates properties of bottom layer.

4.2 Example 2: FGM sandwich plate

Bending behaviour of FGM sandwich plates under thermal loads is studied using semi analytical method. Numerical investigations are carried out on simply supported sandwich square plate under the influence of material gradation in terms of power law index, k, aspect ratio and lamination schemes. FG Material properties used in bending analysis of sandwich plate are shown in Table 3 and lamination schemes are shown in Table 4. The current theory is applied to ceramic-metal FGM sandwich plate consisting of Zirconia (ceramic) at core and Titanium (metal) as the face sheets with FGM material in layers 1 and 3 as shown in Fig. 1. In this plate problem FGM layer material properties varied from Titanium at the face sheet to Zirconia at the core according to

Table 5 Comparison of normalized displacements and stresses of square FGM plate for aspect ratio a/h=10

k	Model	$\bar{u}$		$\bar{w}_{max}$	$\bar{\tau}_{xy}(0,0)$	$\bar{\sigma}_{xx}(a/2,0,z)$		$\bar{\tau}_{xz}(max)$
		$h/2$	$-h/2$		$h/2$	$h/2$	$-h/2$	
0	Present Analysis	-0.167	-1.3494	0.0386	-0.0818	-0.1357	-1.3644	0.4124
	Ref.$^{\$}$	-0.168	-1.372	0.038	-0.081	-0.136	-1.364	0.411
1	Present Analysis	-0.863	-0.1173	0.0256	-0.0567	-0.1776	-2.3478	1.4748
	Ref.$^{\$}$	-0.863	-0.117	0.024	-0.057	-0.180	-2.349	1.473
2	Present Analysis	-0.952	-0.2133	0.0260	-0.1031	-0.0944	-2.1758	0.6104
	Ref.$^{\$}$	-0.952	-0.213	0.026	-0.103	-0.094	-2.176	0.610
4	Present Analysis	-1.122	-0.2834	0.0290	-0.1370	-0.0316	-1.8466	1.0225
	Ref.$^{\$}$	-1.122	-0.283	0.026	-0.137	-0.031	-1.847	1.022
8	Present Analysis	-1.341	-0.296	0.0360	-0.1431	-0.0206	-1.4334	1.5434
	Ref.$^{\$}$	-1.341	-0.296	0.036	-0.143	-0.020	-1.423	1.533

Ref..$^{\$}$: Kulkarni and Pendhari (2021).

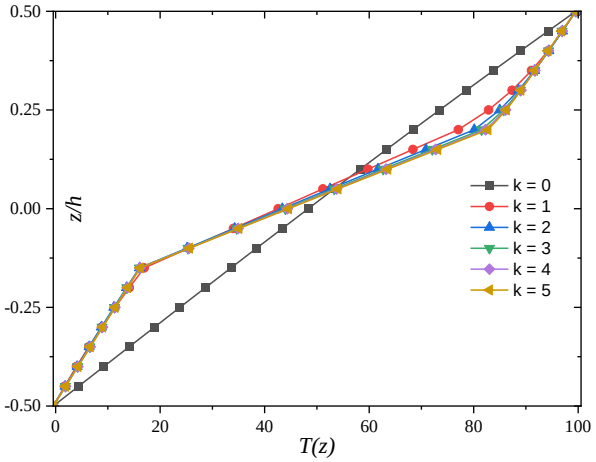

Fig. 3 Through thickness temperature variation for scheme 1-2-1 for $a/h = 10$

power-law distribution in thickness direction (z) and to maintain, the same variation is applied from core to top face. Material properties are varied in terms of power law index ranging from $k = 0$ to 5 accounting the effect of transverse anisotropy/gradation of material. The variation of elastic modulus through the thickness according to power law varying in the range $(k = 1 - 3)$ shows the transition of FG material from ceramic to metal as shown in Fig. 2. The numerical results of displacements and stress are normalized according to Eq. (37).

$$\bar{w} = \frac{h}{a^2\alpha_o\overline{T}_b} w\left(a/2, b/2, 0\right),\ \bar{\sigma}_x = \frac{10h^2}{a^2\alpha_o\overline{T}_b E_0}\sigma_x\left(\frac{a}{2},\frac{b}{2},\frac{h}{2}\right),\ \bar{\tau}_{xz} = \frac{10h}{\alpha_o\overline{T}_b aE_o}\tau_{xz}\left(0,\frac{b}{2},0\right) \tag{37}$$

where E_o=1 GPa, $\alpha_o = 10^{-6}$ K and T_b represent temperature at bottom layer.

The accuracy of the present theory is demonstrated by obtaining the results of displacements and stresses as presented in Table 6 and Fig. 3 and 4 and comparing it with Mechab *et al.* (2010). For determination of through thickness thermal stress variation two models are taken into

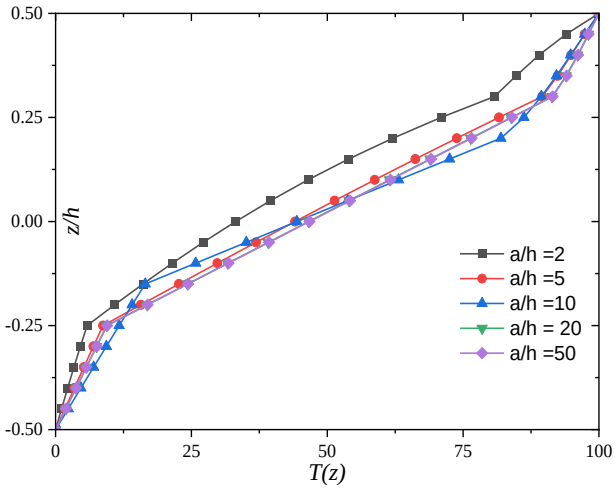

Fig. 4 Through thickness temperature variation for 1-2-1 scheme for $k = 3$

consideration. Model 1 which assumes the temperature profile as linear is compared with Mechab *et al.* (2010) and subsequently the Model 1 is compared with Model 2 which incorporates the actual thermal profile obtained by steady state heat conduction. Variation of temperature through the thickness of sandwich plate obtained is shown in the Figs. 3 and 4 for various values of power law index, k and aspect ratio (a/h).

As seen in Fig. 3 the actual through thickness variation of temperature profile deviates significantly from assumed linear profile because of variation in thermal conductivity of materials. As power law index, k increases the deviation of through thickness temperature profile shows more departure from linear profile. Similarly, from Fig. 4 it is observed that as the plate thickness changes from thick to thin, the through thickness temperature profile becomes piecewise linear i.e., linear in each layer. For very thick plate $(a/h = 2)$ it shows notable departure compared to thin plate.

4.3 Effect of stacking sequence

The normalized central transverse displacement $(\bar{w})$ and axial stress $(\bar{\sigma}_x)$ of square FGM sandwich plate for $a/h = 10$ are presented in Table 6. The through thickness variation of in- plane displacement $(\bar{u})$, transverse displacement $(\bar{w})$, inplane stress $(\bar{\sigma}_x)$, in-plane shear stress $(\bar{\tau}_{xy})$, transverse shear stress $(\bar{\tau}_{xz})$ and transverse normal stress $(\bar{\sigma}_z)$ for different lamination schemes for power law index, $k = 3$ and aspect ratio $a/h = 10$ are shown in Fig. 5. It can be seen from Table 6 that an approximate theory proposed by Tounsi *et al.* (2013) overestimates transverse displacement when compared to model 1 with linear thermal profile.

Through thickness distribution of in-plane displacement $(\bar{u})$ for various lamination schemes is shown in Fig. 5(a). It is seen that the variation of in-plane displacement is linear for moderately thick plate for aspect ratio, $a/h = 10$ and power law index, $k = 3$. This displacement is minimum at the bottom surface and maximum at the top surface. Through thickness distribution of transverse displacement for various lamination schemes is shown in Fig. 5(b). It is seen from this figures that the variation of transverse displacement $(\bar{w})$ is non-linear above the mid surface and

Table 6 Normalized central transverse deflection ($\bar{w}$) and normalized inplane stress ($\bar{\sigma}_x$) for FGM sandwich plate for different schemes for $a/h = 10$ and $a/b = 1$ under thermal load

k	Theory	Scheme							
		1-0-1		1-1-1		1-2-1		2-1-2	
		$\bar{w}$	$\bar{\sigma}_x$	$\bar{w}$	$\bar{\sigma}_x$	$\bar{w}$	$\bar{\sigma}_x$	$\bar{w}$	$\bar{\sigma}_x$
0	Model 1	0.4659	-2.0418	0.4659	-2.0418	0.4659	-2.0418	0.4659	-2.0418
	Model 2	0.4645	-2.0795	0.4645	-2.0795	0.4645	-2.0795	0.4645	-2.0795
	Ref.*	0.4803	-2.0796	0.4803	-2.0796	0.4803	-2.0796	0.4803	-2.0796
1	Model 1	0.6183	-2.0791	0.5881	-2.2380	0.5618	-2.3421	0.6031	-2.1672
	Model 2	0.6917	-1.9820	0.7062	-2.0437	0.6711	-2.1560	0.7142	-1.9833
	Ref.*	0.6369	-1.9939	0.6062	-2.1444	0.5823	-2.2620	0.6211	-2.0716
2	Model 1	0.6537	-1.9236	0.6193	-2.1239	0.5848	-2.2638	0.6371	-2.0318
	Model 2	0.7198	-1.8307	0.7558	-1.8747	0.7098	-2.0324	0.7615	-1.8012
	Ref.*	0.6715	-1.8242	0.6393	-1.9822	0.6098	-2.1272	0.6561	-1.8997
3	Model 1	0.6651	-1.8563	0.6324	-2.0736	0.5938	-2.2321	0.6508	-1.9711
	Model 2	0.7234	-1.7718	0.7746	-1.8030	0.7242	-1.9838	0.7773	-1.7240
	Ref.*	0.6836	-1.7647	0.6564	-1.9120	0.6224	-2.0654	0.6703	-1.8302
4	Model 1	0.6699	-1.8202	0.6391	-2.0467	0.5980	-2.2166	0.6576	-1.9375
	Model 2	0.7228	-1.7417	0.7835	-1.7661	0.7307	-1.9608	0.7838	-1.6835
	Ref.*	0.6888	-1.7389	0.6613	-1.8745	0.6295	-2.0308	0.6773	-1.7956
5	Model 1	0.6701	-1.7982	0.6429	-2.0305	0.6002	-2.2083	0.6614	-1.9165
	Model 2	0.7197	-1.7239	0.7882	-1.7448	0.7341	-1.9485	0.7869	-1.6592
	Ref.*	0.6914	-1.7260	0.6659	-1.8519	0.6340	-2.0088	0.6813	-1.7757

Ref.* : Tounsi *et al.* (2013)

almost constant below it. As the core thickness decreases, a notable increase in deflection occurs because of decrease in the plate's stiffness. Fig. 5(c) shows through thickness variation of inplane stress ($\bar{\sigma}_x$), and its variation in non-linear in bottom and top face sheets while it is linear in core thickness. In the interface of bottom face sheet and core it is characterized by kink due to lower temperature for all lamination schemes. Variation of in plane shear stress for all stacking sequences at $a/h = 10$ and $k = 3$ is non-linear across thickness above the mid surface whereas it is nearly constant below the mid surface of the sandwich plate as seen in Fig. 5(d).

The variation of transverse shear stress ($\bar{\tau}_{xz}$) is shown in Fig. 5(e) for various schemes. The variation in each scheme of sandwich plate is parabolic through the thickness, however it is antisymmetric (changes sign) with respect to midplane. It shows maximum values at the interface between the core and face sheet and satisfies surface constraints at the top and bottom surfaces. Variation of transverse normal stress ($\bar{\sigma}_z$) through thickness is shown is Fig. 5(f). It shows maximum value at the vicinity of mid surface of core. The nature of variation is distinct for each scheme of lamination indicating the effect of thickness of each layer. As the core thickness increases it becomes symmetric with respect to the mid surface of the sandwich plate. In absence of transverse load, the variation of this stress satisfies the vanishing surface constraints at bounding planes.

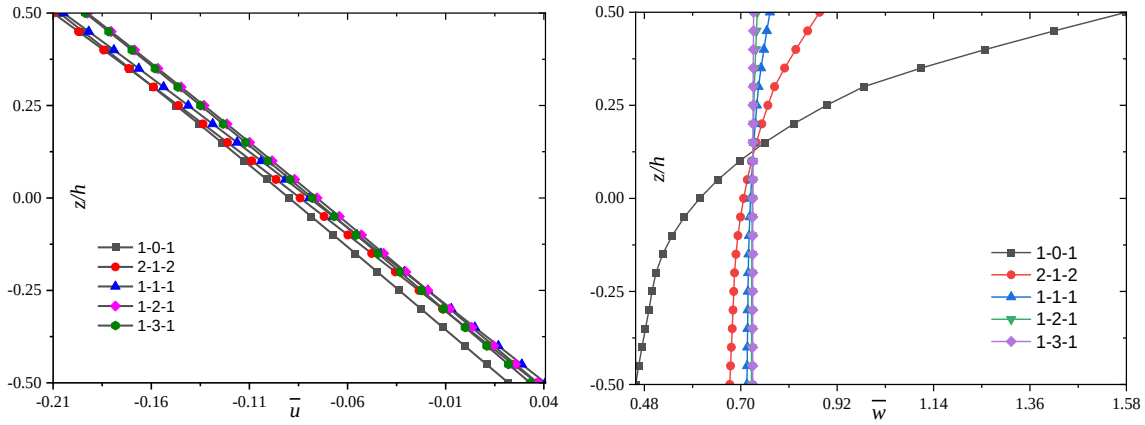

(a) In-plane displacement (b) Transverse displacement

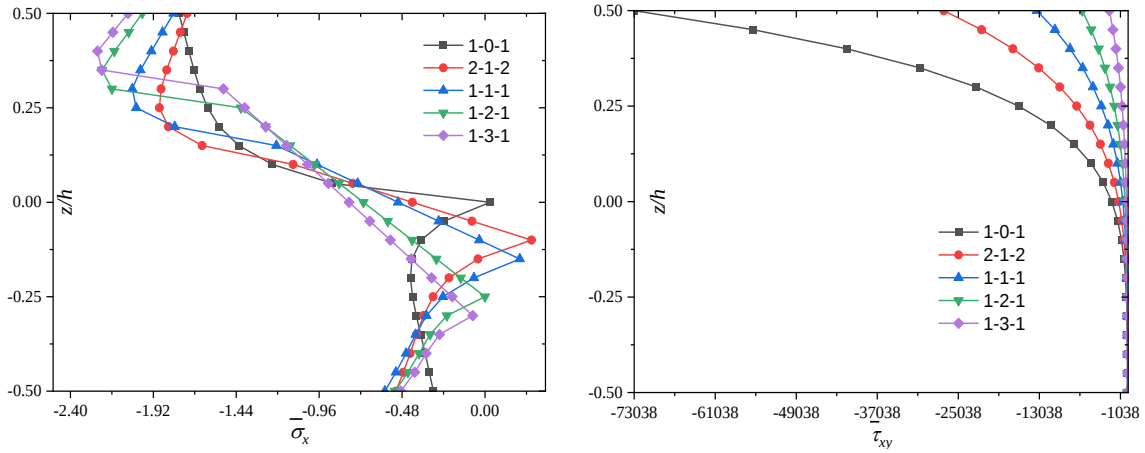

(c) In-plane normal stress (d) In-plane shear stress

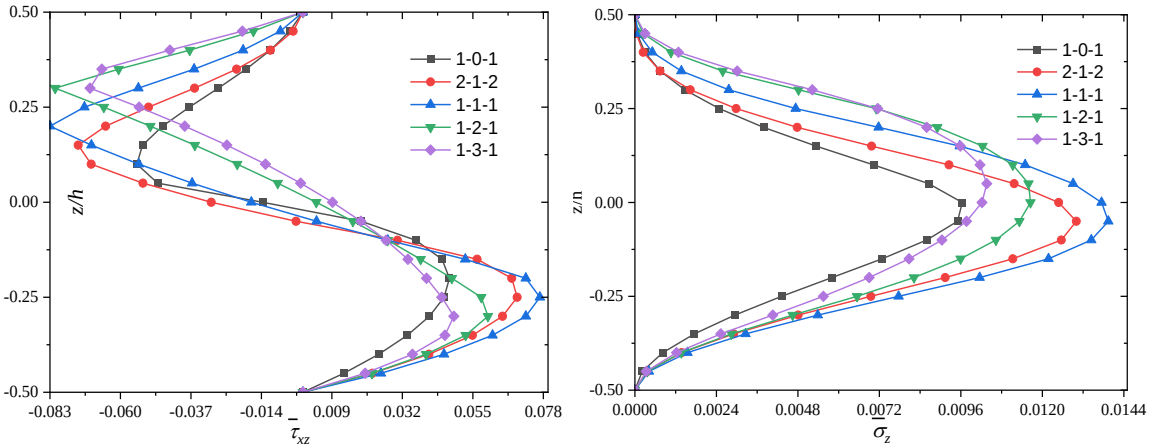

(e)Transverse shear stress (f) Transverse normal stress

Fig. 5 Through thickness variations of displacements and stresses for different schemes at $k = 3$ and $a/h = 10$

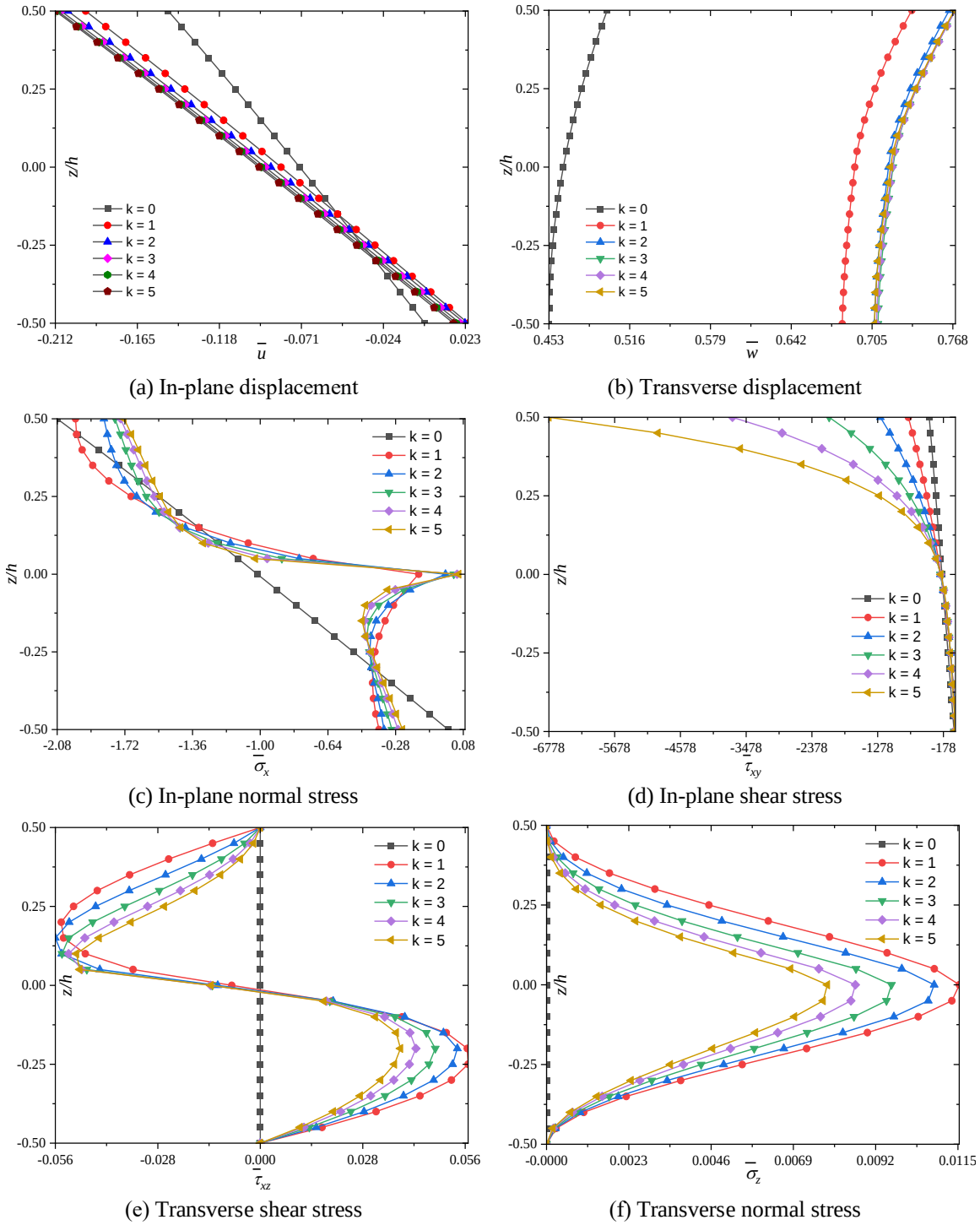

(a) In-plane displacement

(b) Transverse displacement

(c) In-plane normal stress

(d) In-plane shear stress

(e) Transverse shear stress

(f) Transverse normal stress

Fig. 6 Through thickness variations of displacements and stresses for various inhomogeneity indices for 1-0-1 stacking sequence of square sandwich plate with $a/h = 10$

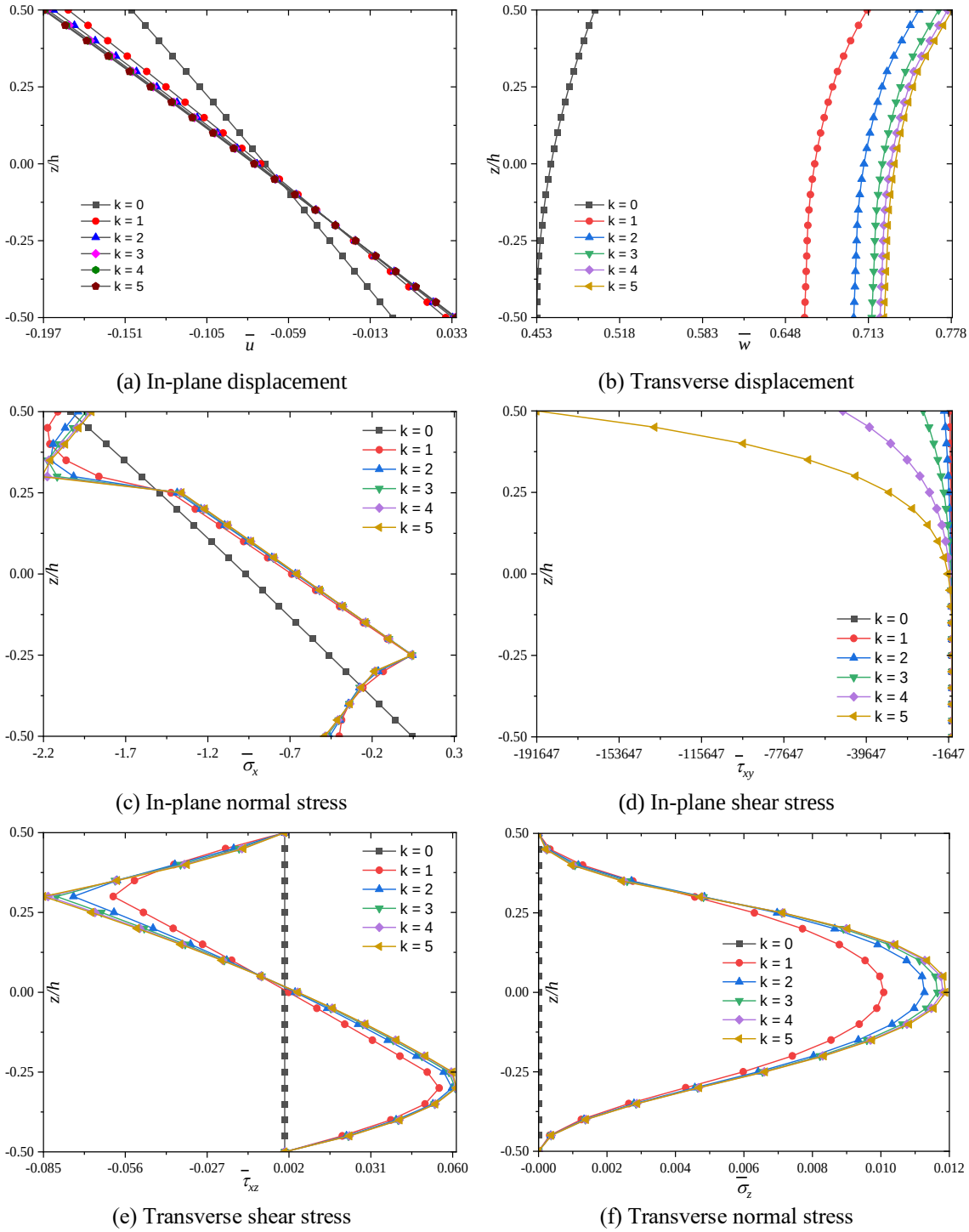

(a) In-plane displacement

(b) Transverse displacement

(c) In-plane normal stress

(d) In-plane shear stress

(e) Transverse shear stress

(f) Transverse normal stress

Fig. 7 Through thickness variations of displacements and stresses for various inhomogeneity indices for 1-2-1 stacking sequence of square sandwich plate with $a/h = 10$

Table 7 Normalized transverse displacement ($\bar{w}$), shear stress ($\bar{\tau}_{xz}$) and in-plane stress ($\bar{\sigma}_x$) for different schemes and aspect ratios *S* of square sandwich plate according to heat conduction thermal profile

S	k	Parameters	Scheme			
			1-0-1	1-1-1	1-2-1	2-1-2
2	0	$\bar{w}$	0.3846	0.3846	0.3846	0.3846
		$\bar{\tau}_{xz}$	-0.0004	-0.0004	-0.0004	-0.0004
		$\bar{\sigma}_x$	-10.4000	-10.4000	-10.4000	-10.4000
	1	$\bar{w}$	0.5690	0.5793	0.5641	0.5787
		$\bar{\tau}_{xz}$	-0.9834	-1.2790	0.1136	-1.9518
		$\bar{\sigma}_x$	-9.0378	-9.0912	-9.6256	-8.9013
	2	$\bar{w}$	0.5833	0.6139	0.5969	0.6068
		$\bar{\tau}_{xz}$	-1.3800	-1.6026	0.2891	-2.6284
		$\bar{\sigma}_x$	-8.4458	-8.2356	-8.8901	-8.0803
	3	$\bar{w}$	0.5818	0.6247	0.6080	0.6128
		$\bar{\tau}_{xz}$	-1.5246	-1.7931	0.3382	-2.9902
		$\bar{\sigma}_x$	-8.2999	-7.9263	-8.6243	-7.8070
	4	$\bar{w}$	0.5789	0.6287	0.6125	0.6135
		$\bar{\tau}_{xz}$	-1.5558	-1.9100	0.3528	-3.1996
		$\bar{\sigma}_x$	-8.2533	-7.7855	-8.5051	-7.6909
	5	$\bar{w}$	0.5763	0.6303	0.6147	0.6129
		$\bar{\tau}_{xz}$	-1.5396	-1.9853	0.3572	-3.3298
		$\bar{\sigma}_x$	-8.2356	-7.7117	-8.4442	-7.6334
20	0	$\bar{w}$	0.4673	0.4673	0.4673	0.4673
		$\bar{\tau}_{xz}$	0.0000	0.0000	0.0000	0.0000
		$\bar{\sigma}_x$	-1.0400	-1.0400	-1.0400	-1.0400
	1	$\bar{w}$	0.6960	0.7107	0.6749	0.7190
		$\bar{\tau}_{xz}$	-0.0010	-0.0015	0.0002	-0.0023
		$\bar{\sigma}_x$	-0.9949	-1.0267	-1.0827	-0.9962
	2	$\bar{w}$	0.7227	0.7609	0.7138	0.7670
		$\bar{\tau}_{xz}$	-0.0015	-0.0019	0.0005	-0.0032
		$\bar{\sigma}_x$	-0.9187	-0.9424	-1.0214	-0.9050
	3	$\bar{w}$	0.7264	0.7799	0.7282	0.7832
		$\bar{\tau}_{xz}$	-0.0016	-0.0021	0.0006	-0.0038
		$\bar{\sigma}_x$	-0.8887	-0.9066	-0.9974	-0.8661
	4	$\bar{w}$	0.7260	0.7890	0.7349	0.7901
		$\bar{\tau}_{xz}$	-0.0017	-0.0023	0.0006	-0.0041
		$\bar{\sigma}_x$	-0.8732	-0.8880	-0.9859	-0.8455
	5	$\bar{w}$	0.7248	0.7939	0.7383	0.7933
		$\bar{\tau}_{xz}$	-0.0017	-0.0024	0.0006	-0.0043
		$\bar{\sigma}_x$	-0.8640	-0.8773	-0.9798	-0.8332

4.4 Effect of transverse anisotropy (k)

The through-the-thickness variation of in-plane displacement ($\bar{u}$), transverse displacement ($\bar{w}$),

in-plane stress ($\bar{\sigma}_x$), in-plane shear stress transverse $(\bar{\tau}_{xy})$, transverse shear stress ($\bar{\tau}_{xz}$) and transverse stress ($\bar{\sigma}_z$) for different power law index, k for lamination schemes 1-0-1 and 1-2-1 and aspect ratio 10 are plotted in Figs. 6 and 7 respectively.

Through thickness distribution of in-plane displacement ($\bar{u}$) for various power law indices is shown in Figs. 6(a) and 7(a). It is seen that the variation of in-plane displacement is linear for moderately thick plate for aspect ratio, $a/h = 10$ for both lamination schemes. This displacement is minimum at the bottom surface and maximum at the top surface and displacement at the top surface increases with increase with power law index and variations show close proximity after power index, $k = 3$. Through thickness distribution of transverse displacement for various power law index is shown in Figs. 6(b) and 7(b). It is seen that the variation of transverse displacement ($\bar{w}$) is non-linear above the mid surface and almost constant below it. With increase in power law index the transverse displacement increases due to decrease in transverse anisotropy. Figs. 6(c) and 7(c) show the through the thickness variations of axial stress ($\bar{\sigma}_x$). This stress variation is non-linear in bottom and top FGM face sheets due to gradation in material properties while it is linear in core thickness being isotropic. This stress shows maximum value at the interface and increases with increase in power law index, k and shows tensile and compressive natures in each FGM layer. At the interface of bottom face sheet and core it is characterized by kink due to high thermal gradient. The variation of in plane shear stress $(\bar{\tau}_{xy})$ for all power law indices from 0 to 5 at $a/h = 10$ and stacking scheme 1-0-1 and 1-2-1 is non-linear across thickness above the mid surface whereas it is nearly constant below the mid surface of the sandwich plate as seen in Figs. 6(d) and 7(d). The variation of transverse shear stress ($\bar{\tau}_{xz}$) is shown in Figs. 6(e) and 7(e). It is parabolic and anti-symmetric in nature through the thickness showing maximum values this stress at the interface. The value of this stress at the interface between the core and the face sheet increases with increase in inhomogeneity factor and satisfies the continuity condition at the interface and the surface constraints at the top and bottom surfaces of the plate. The variation of transverse normal stress ($\bar{\sigma}_z$) through thickness is shown in Figs. 6(f) and 7(f) satisfying the zero load conditions on the bounding plane of the plate. The variation is symmetric about the mid surface of the FGM sandwich plate. It shows maximum value of this stress to occur at the mid surface or neutral surface which increases with increase in k without shift in the position in transverse direction.

4.5 Effect of aspect ratio (a/h)

Table 7 shows the maximum values of displacement and stress for all stacking schemes for all power law indices and aspect ratios 2 and 20. For thick plate, S=2 and lamination scheme (1-0-1) transverse displacement ($\bar{w}$) increases with increase in power law index k up to 4 whereas for schemes (1-1-1) and (1-2-1), it increased for all values of power law index. This variation in this displacement is attributed to degree of transverse anisotropy and the flexural stiffness of the FGM sandwich plate. The transverse shear stress ($\bar{\tau}_{xz}$) is found to increase with increase in value of k for all lamination schemes. Among all the schemes the scheme (2-1-2) is found to yield highest values of this stress for all values of k for both the aspect ratios 2 and 20. The inplane stress ($\bar{\sigma}_x$) is found decrease with increase in power law index for all the schemes due to increase in metal phase.

The through thickness variation of in-plane displacement ($\bar{u}$), transverse displacement ($\bar{w}$), axial stress ($\bar{\sigma}_x$), in-plane shear stress transvers $(\bar{\tau}_{xy})$, transverse shear stress ($\bar{\tau}_{xz}$) and transverse

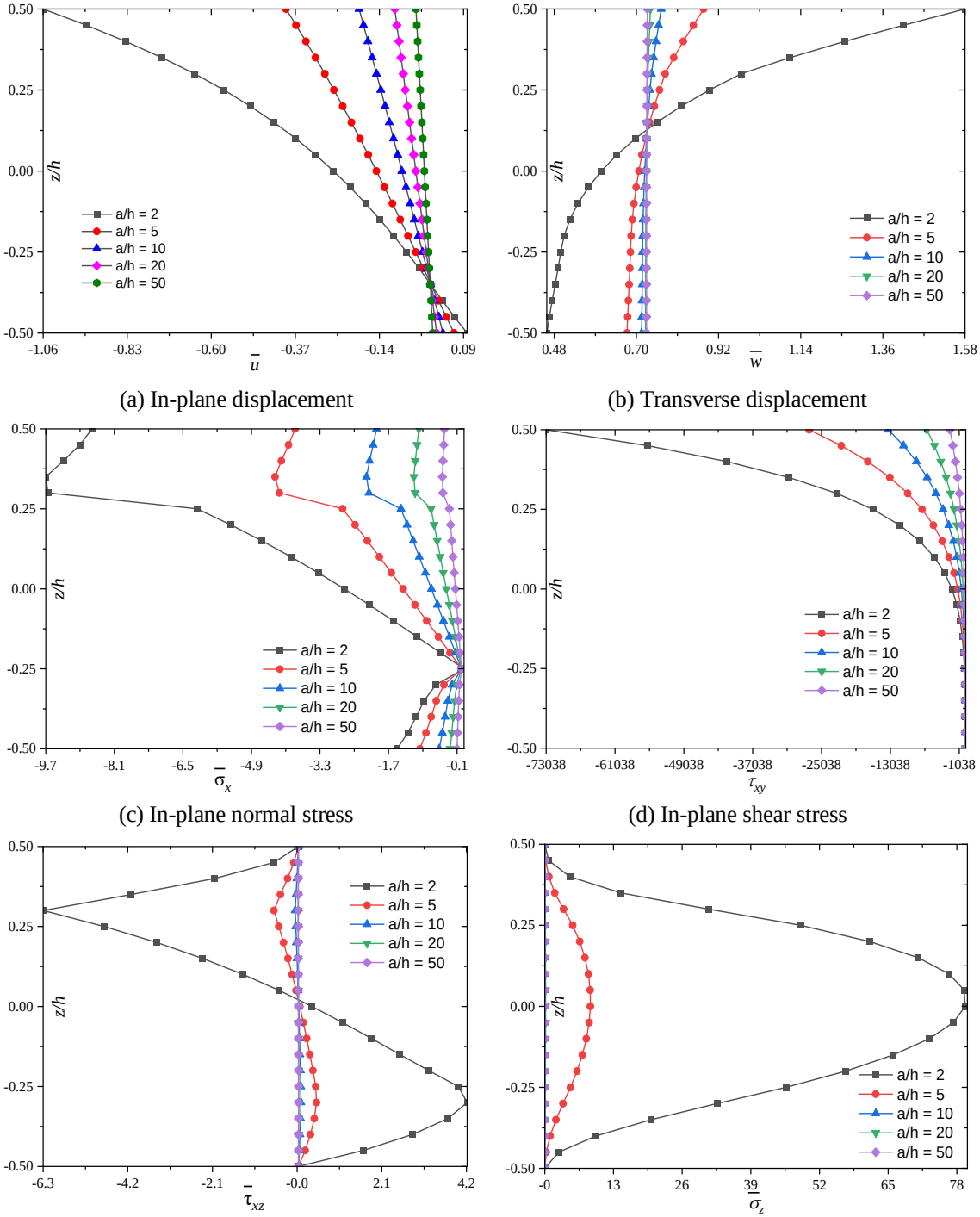

(a) In-plane displacement (b) Transverse displacement

(c) In-plane normal stress (d) In-plane shear stress

(e) Transverse shear stress (f) Transverse normal stress

Fig. 8 Through thickness variations of displacements and stresses of sandwich plate with stacking scheme 1-2-1 with aspect ratio (a/h) with material inhomogeneity index $k = 3$

stress ($\bar{\sigma}_z$) for power law index, $k = 3$ for lamination scheme (1-2-1) for different aspect ratio are shown in Fig. 8. Through the thickness distributions of displacements and stresses show significant departure for very thick plate ($a/h = 2$) compared to higher aspect ratio ($a/h = 50$) because of predominant shear and normal deformations in thick plate. The inplane displacement ($\bar{u}$) variation across the thickness of plate shows maximum value at top surface and minimum at the bottom surface for all aspect ratios. This displacement is maximum for very thick FGM sandwich plate.

The inplane displacement ($\bar{u}$) variations for all aspect ratios are found to have common point of intersection at $z = -3h/8$ below the mid plane as seen from Fig. 8(a). The variation of transverse displacement as shown in Fig. 8(b) indicates maximum value at top surface (ceramic) and minimum at the bottom surface (metal). The variation of this displacement for very thick plate, *S*=2 shows great departure compared to those of other aspect ratios from *S*=5 to 50 due to attenuation in shear and normal deformation effects with increase in aspect ratio. All the distribution curves of this displacement pass through the common point of intersection at $z = +h/8$ above the mid plane.

In-plane stress ($\bar{\sigma}_x$) as shown in Fig. 8(c) is maximum at top surface and minimum at bottom layer interface between core and face sheet due to attenuation in rate of heat transfer from top surface to bottom surface and gradient in material properties. It shows non-linear behaviour for all aspect ratios, and it is completely compressive in FGM face sheets and middle core. In core its variation is linear whereas it is nonlinear in FGM face sheets. The variation of inplane shear stress $(\bar{\tau}_{xy})$ across the thickness is almost constant below the mid surface symmetric (1-2-1) FGM sandwich plate as revealed in Fig. 8(d) whereas it is nonlinear above the mid surface and shows maximum value at top surface (ceramic) with immediate vicinity of thermal front at $z = +h/2$ for all aspect ratios.

The variation of transverse shear stress shown in Fig. 8(e) is antisymmetric with reference to mid plane and parabolic in nature in bottom FGM face sheet and concave parabolic in top FGM face sheet for thick plate with *S*=2. For moderately thick to thin plates (*S*=10-50) the variations are coinciding with each other. The variation of this stress through the thickness satisfies surface constraints and continuity condition at the interfaces. The transverse norm stress ($\bar{\sigma}_z$) variation across the thickness of plate is shown in Fig. 8(f). The variation is symmetric with respect to the mid plane and shows maximum value at *z*=0 and zero values at top and bottom surfaces satisfying the zero normal traction at the bounding planes. The variation of this stress across the thickness of FGM sandwich plate satisfies the continuity condition at the interface between the layers of dissimilar materials for all aspect ratios.

5. Conclusions

This study conducts a pure thermal bending analysis of a functionally graded (FG) sandwich plate using a semi-analytical method. The semi analytical method developed within the framework of linear theory of elasticity. Thermal profile is derived using Fourier's law of heat conduction under steady state condition. FGM sandwich plate material properties such as modulus of elasticity (E), thermal coefficient of expansion (α) and thermal conductivity (λ) are varied according to power law. The power law index which represents degree of transverse anisotropy/inhomogeneity is varied from 0 to 5. Boundary value problem (BVP) is converted to initial value problem (IVP)

using shooting method. Thermo-flexural response is validated with existing solution for FGM plate. The influence of stacking sequence, material inhomogeneity and aspect ratio are examined for FGM sandwich plate. Exact elasticity solution for FGM sandwich plate in which material properties vary according to power law does not exist due mathematical limitations. Thus, in the absence of exact elasticity solutions present semi-analytical solution can be treated as exact solution which can be used as a benchmark solution to validate approximate solutions.

References

Alibeigloo, A. (2017), "Three-dimensional coupled thermo-elasticity solution of sandwich plate with FGM core under thermal shock", *Compos. Struct*., **177**, 96-103. https://doi.org/10.1016/j.compstruct.2017.06.046.

Alimohammadi Madanouei, I. and Karamooz Mahdiabadi, M. (2024), "Free and forced vibration mitigation of nonlinear functionally graded beams based on higher-order shear deformation theories using NES*", Int. J. Struct. Stab. Dyn*., 2550244. https://doi.org/10.1142/S021945542550244X.

Benameur, I., Beldjelili, Y. and Tounsi, A. (2023), "Analytical and finite element method for the bending analysis of the thick porous functionally graded sandwich plate including thickness stretching effect", *Struct. Eng. Mech*., **85**(5), 593-605. https://doi.org/10.12989/sem.2023.85.5.593.

Benguediab, S., Kebir, T., Kettaf, F.Z., Daikh, A.A., Tounsi, A., Benguediab, M. and Eltaher, M.A. (2023), "Thermomechanical behavior of macro and nano fgm sandwich plates", *Adv. Aircraft Spacecraft Sci*., **10**(1), 83-106. https://doi.org/10.12989/aas.2023.10.1.083.

Boley, B.A., Weiner, J.H. (1960), *Theory of Thermal Stresses*, John Wiley, New York, USA.

Carslaw, H.S. and Jaeger, J.C. (1947), *Conduction of Heat in Solids*, Oxford University Press, New York.

Chitour, M., Benguediab, S., Bouhadra, A., Bourada, F., Benguediab, M. and Tounsi, A. (2024), "Effect of variable volume fraction distribution and geometrical parameters on the bending behavior of sandwich plates with FG isotropic face sheets", *Mech. Bas. Des. Struct. Mach*., **52**, 3079-3105. https://doi.org/10.1080/15397734.2023.2197036.

Dadashi, M. and Mahdiabadi, M.K. (2024), "Dynamic analysis of functionally graded sandwich doubly curved nanoshells using variable nonlocal elasticity theory", *Int. J. Struct. Stab. Dyn*., **25**, 2550122. https://doi.org/10.1142/S0219455425501226.

Desai, P. and Kant, T. (2015), "On numerical analysis of axisymmetric thick circular cylindrical shells based on higher order shell theories by segmentation method", *J. Sandw. Struct. Mater*., **17**(2), 130-169. https://doi.org/10.1177/1099636214554905.

Di Sciuva, M. and Sorrenti, M. (2021), "Bending and free vibration analysis of functionally graded sandwich plates: An assessment of the refined zigzag theory", *J. Sandw. Struct. Mater*., **23**, 760-802. https://doi.org/10.1177/1099636219843970.

Garg, A., Belarbi, M.O., Chalak, H.D. and Chakrabarti, A. (2021), "A review of the analysis of sandwich FGM structures", *Compos. Struct*., **258**, 113427. https://doi.org/10.1016/j.compstruct.2020.113427.

Hajlaoui, A., Chebbi, E. and Dammak, F. (2021), "Three-dimensional thermal buckling analysis of functionally graded material structures using a modified FSDT-based solid-shell element", *Int. J. Press. Ves. Pip*., **194**, 104547. https://doi.org/10.1016/j.ijpvp.2021.104547.

Hamidi, A., Houari, M.S.A., Mahmoud, S.R. and Tounsi, A. (2015), "A sinusoidal plate theory with 5-unknowns and stretching effect for thermomechanical bending of functionally graded sandwich plates", *Steel Compos. Struct*., **18**(1), 235-253. https://doi.org/10.12989/scs.2015.18.1.235.

Himeur, N., Mamen, B., Benguediab, S., Bouhadra, A., Menasria, A., Bouchouicha, B., Bourada, F. and Benguediab, M. (2022), "Coupled effect of variable Winkler-Pasternak foundations on bending behavior of FG plates exposed to several types of loading", *Steel Compos. Struct*., **44**(3), 353-369. https://doi.org/10.12989/scs.2022.44.3.353.

Ingersoll, L.R., Zobel, O.J. and Ingersoll, A.C. (1948), *Heat Conduction*, McGraw-Hill Book Co., New

York.
Jin, Z.H. and Paulino, G.H. (2000), "Transient thermal stress analysis of an interior crack in functionally graded materials", *Proceedings of the ASME 2000 International Mechanical Engineering Congress and Exposition. Adaptive Structures and Material Systems*, Orlando, Florida, November. https://doi.org/10.1115/IMECE2000-1697.
Jones, R.M. (1975), *Mechanics of Composite Materials*, 2nd Edition, Taylor & Francis, Inc., Philadelphia.
Kant, T., Gupta, A.B., Pendhari, S.S. and Desai, Y.M. (2008), "Elasticity solution for cross-ply composite and sandwich laminates", *Compos. Struct*., **83**, 13-24. https://doi.org/10.1016/j.compstruct.2007.03.003.
Koizumi, M. (1997), "FGM activities in Japan", *Compos. Part B Eng*., **28**(1-2), 1-4. https://doi.org/10.1016/S1359-8368(96)00016-9.
Kulkarni, S.P. and Pendhari, S.S. (2021), "3D Semi-analytical solutions for functionally grade power law varied laminate subjected to thermo-mechanical loading", *J. Comput. Eng. Phys. Model*., **4**(3), 70-98. https://doi.org/10.22115/CEPM.2021.265578.1148.
Li, M., Chen, C.S., Chu, C.C. and Young, D.L. (2014), "Transient 3D heat conduction in functionally graded materials by the method of fundamental solutions", *Eng. Anal. Bound. Elem*., **45**, 62-67. https://doi.org/10.1016/j.enganabound.2014.01.019.
Madanouei, A.I. and Mahdiabadi, M.K. (2024), "Free and forced vibration mitigation of nonlinear functionally graded beams based on higher-order shear deformation theories using NES", *Int. J. Struct. Stab. Dyn*., 2550244. https://doi.org/10.1142/S021945542550244X.
Malek, M., Izem, N., Mohamed, M.S. and Seaid, M. (2020), "A three-dimensional enriched finite element method for nonlinear transient heat transfer in functionally graded materials", *Int. J. Heat Mass Trans*., **155**, 119804. https://doi.org/10.1016/j.ijheatmasstransfer.2020.119804.
Mechab, I., Atmane, H.A., Tounsi, A., Belhadj, H.A. and Bedia, E.A.A. (2010), "A two variable refined plate theory for the bending analysis of functionally graded plates", *Acta Mechanica Sinica*, **26**(6), 941-949. https://doi.org/10.1007/s10409-010-0372-1.
Naghavi, M., Sarrami-Foroushani, S. and Azhari, F. (2022), "Bending analysis of functionally graded sandwich plates using the refined finite strip method", *J. Sandw. Struct. Mater*., **24**(1), 448-483. https://doi.org/10.1177/10996362211020448.
Neves, A.M.A., Ferreira, A.J.M., Carrera, E., Cinefra, M., Roque, C.M.C., Jorge, R.M.N. and Soares, C.M.M. (2013), "Static, free vibration and buckling analysis of isotropic and sandwich functionally graded plates using a quasi-3D higher-order shear deformation theory and a meshless technique", *Compos. Part B Eng*., **44**, 657-674. https://doi.org/10.1016/j.compositesb.2012.01.089.
Ootao, Y. and Tanigawa, Y. (1999), "Three-dimensional transient thermal stresses of functionally graded rectangular plate due to partial heating", *J. Therm. Stress*., **22**(1), 35-55. https://doi.org/10.1080/014957399281048.
Özışık, M.N. (1989), *Boundary Value Problems of Heat Conduction*, 1st Edition, Dover Publications, New York.
Pandey, S. and Pradyumna, S. (2018), "Analysis of functionally graded sandwich plates using a higher-order layerwise theory", *Compos. Part B Eng*., **153**, 325-336. https://doi.org/10.1016/j.compositesb.2018.08.121.
Sankar, B.V. and Tzeng, J.T. (2002), "Thermal stresses in functionally graded beams", *AIAA J*., **40**, 1228-1232. https://doi.org/10.2514/2.1775.
Sayyad, A.S. and Ghugal, Y.M. (2021), "A unified five-degree-of-freedom theory for the bending analysis of softcore and hardcore functionally graded sandwich beams and plates", *J. Sandw. Struct. Mater*., **23**, 473-506. https://doi.org/10.1177/1099636219840980.
Shao, Z.S., Wang, T.J. and Ang, K.K. (2007), "Transient thermomechanical stresses of functionally graded cylindrical panels", *AIAA J*., **45**, 2487-2496. https://doi.org/10.2514/1.24328.
Shiota, I. and Miyamoto, Y. (1997), *Functionally Graded Materials 1996*, Elsevier Science, Tokyo, Japan.
Slimani, R., Menasria, A., Ali Rachedi, M., Mourad, C., Refrafi, S., Nimer, A.A., Bouhadra, A. and Mamen, B. (2024), "A novel quasi-3D refined HSDT for static bending analysis of porous functionally graded plates", *J. Comput. Appl. Mech*., **55**, 519-537. https://doi.org/10.22059/jcamech.2024.372417.968.

Tamrabet, A., Mamen, B., Menasria, A., Bouhadra, A., Tounsi, A., Ghazwani, M.H., Alnujaie, A. and Mahmoud, S.R. (2023), "Buckling behaviors of FG porous sandwich plates with metallic foam cores resting on elastic foundation", *Struct. Eng. Mech.*, **85**(3), 289-304. https://doi.org/10.12989/sem.2023.85.3.289.

Tamrabet, A., Mourad, C., Ali Alselami, N., Menasria, A., Mamen, B. and Bouhadra, A. (2024), "Efficient kinematic model for stability analysis of imperfect functionally graded sandwich plates with ceramic middle layer and varied boundary edges", *J. Comput. Appl. Mech.*, **55**, 184-200. https://doi.org/10.22059/jcamech.2024.371464.947.

Tounsi, A., Houari, M.S.A., Benyoucef, S. and Adda Bedia, E.A. (2013), "A refined trigonometric shear deformation theory for thermoelastic bending of functionally graded sandwich plates", *Aerosp. Sci. Tech.*, **24**, 209-220. https://doi.org/10.1016/j.ast.2011.11.009.

Vel, S.S. and Batra, R.C. (2002), "Exact solution for thermoelastic deformations of functionally graded thick rectangular plates", *AIAA J.*, **40**(7), 1421-1433. https://doi.org/10.2514/2.1805.

Vel, S.S. and Batra, R.C. (2003), "Three-dimensional analysis of transient thermal stresses in functionally graded plates", *Int. J. Solid. Struct.*, **40**(25), 7181-7196. https://doi.org/10.1016/S0020-7683(03)00361-5.

Yadav, S.S., Damse, S., Pendhari, S.S., Sangle, K.K. and Sayyad, A.S (2022), "Comparative studies between semi-analytical and shear deformation theories for functionally graded beam under bending", *Forc. Mech.*, **8**, 100111. https://doi.org/10.1016/j.finmec.2022.100111.

Yadav, S.S., Sangle, K.K., Kokane, U.K., Pendhari, S.S. and Ghugal, Y.M. (2023), "Bending analysis of exponentially varied FG plates using trigonometric shear and normal deformation theory", *Adv. Aircraft Spacecraft Sci.*, **10**(3), 281. https://doi.org/10.12989/aas.2023.10.3.281.

Yadav, S.S., Sangle, K.K., Shinde, S.A., Pendhari, S.S. and Ghugal, Y.M. (2023), "Bending analysis of FGM plates using sinusoidal shear and normal deformation theory", *Forc. Mech.*, **11**, 100185. https://doi.org/10.1016/j.finmec.2023.100185.

Zenkour, A.M. (2005), "A comprehensive analysis of functionally graded sandwich plates: Part 1-Deflection and stresses", *Int. J. Solid. Struct.*, **42**, 5224-5242. https://doi.org/10.1016/j.ijsolstr.2005.02.015.

Zhi-He, J. and Naotake, N. (1994), "Transient thermal stress intensity factors for a crack in a semi-infinite plate of a functionally gradient material", *Int. J. Solid. Struct.*, **31**, 203-218. https://doi.org/10.1016/0020-7683(94)90050-7.

Zohra, A., Rabia, B. and Tahar, H.D. (2023), "Critical thermal buckling analysis of porous FGP sandwich plates under various boundary conditions", *Struct. Eng. Mech.*, **87**(1), 29-46. https://doi.org/10.12989/sem.2023.87.1.029.

CC